

## LiMn<sub>2-x</sub>Ni<sub>x</sub>O<sub>4</sub> Spinel Oxides as High-Temperature Lithium Battery Cathode Materials for Borehole Applications

Zhenjie Wang<sup>1,2</sup>, Junlin Du<sup>1,2</sup>, Weiyuan Duan<sup>1,2</sup>, Yongqiang Niu<sup>1,2</sup>, Zhu Wu<sup>1,\*</sup>

<sup>1</sup> Research center for new energy technology, Shanghai Institute of Microsystem and Information Technology, Chinese Academy of Sciences, Shanghai 201800, China

<sup>2</sup> University of Chinese Academy of Sciences, Beijing 100039, China

\*E-mail: [wuzhu@mail.sim.ac.cn](mailto:wuzhu@mail.sim.ac.cn)

Received: 22 March 2013 / Accepted: 13 April 2013 / Published: 1 May 2013

---

LiMn<sub>2</sub>O<sub>4</sub> and its Ni-substituted derivative electrodes are successfully introduced to high-temperature lithium batteries for borehole applications. The samples prepared by a sol-gel method each have a single spinel-phase, small particle size of 100-200 nm, and excellent discharge capacity. The original LiMn<sub>2</sub>O<sub>4</sub> cathode presents three characteristic voltage plateaux at 2.65-2.55V, 2.15-1.75V and 1.70V-1.00V and a maximum discharge capacity of 459.57 mAh·g<sup>-1</sup> to a 1.00V cut-off at 250 °C under 10mA·cm<sup>-2</sup> constant current discharge. Also, the corresponding reaction mechanisms are investigated by means of XRD method. In general, the better morphology, more stable voltage plateaux and higher discharge capacities are obtained by partly substituting Ni for Mn. Due to these properties, the Ni-substituted LiMn<sub>2</sub>O<sub>4</sub> cathodes are believed to be promising for the progress of the high-temperature lithium battery technology.

---

**Keywords:** Spinel lithium manganate; Nickel substitution; High-temperature lithium primary batteries; Borehole applications; High energy density

### 1. INTRODUCTION

Power sources used in boreholes for geothermal and oil/gas exploration are usually primary batteries, which are low-current so-called “keep-alive” applications for memory retention in the MWD (Measure While Drilling) data logger [1]. At present, modified Li-Mg/SOCl<sub>2</sub> cells are the main solution for these applications [2], but this technology is usually limited below 200 °C due to the low decomposition temperature of SOCl<sub>2</sub> and high vapor pressure inside batteries at higher temperatures. To solve these problems, expensive vacuum dewars are always coupled with Li-Mg/SOCl<sub>2</sub> cells at

higher operating temperatures even above 300 °C which results to higher production costs significantly.

Thermal batteries are widely used for weapons and missile applications which are activated by an internal pyrotechnic and operate between 350 and 550 °C [3]. Molten salt electrolytes in thermal batteries provide excellent ionic conductivity and long lifetime, because they are inert in the storage period which reduces self-discharge effectively. Due to these advantages, much attention is paid to introducing thermal battery technology into geothermal and oil/gas borehole applications. The main problems are concentrated in how to eliminate the expensive dewar and internal pyrotechnic and use the heat of the borehole to maintain the electrolyte in the molten state at temperatures of above 200 °C [4].

Compared with LiCl-KCl eutectic (m.p.=352 °C) electrolyte usually used in thermal batteries, nitrate eutectics, especially LiNO<sub>3</sub>-KNO<sub>3</sub> eutectic which melts at a much lower temperature of 124.5 °C is quite suitable for the geothermal and oil/gas exploration environment, because it can melt automatically by the use of the heat of the borehole. Miles and Giwa studied various cell combinations coupled with this eutectic and verified its applicability [5-7]. Serious exothermic reactions occur between nitrate electrolytes and traditional FeS<sub>2</sub> and CoS<sub>2</sub> cathodes used in thermal batteries. So it is necessary to find other suitable cathode materials. Spinel LiMn<sub>2</sub>O<sub>4</sub> coupled with Li-Si anode and CsBr-LiBr-KBr eutectic electrolyte exhibited a flat plateau voltage of 2.7 V and a capacity of almost 400 C·g<sup>-1</sup> [8]. Bolster et al. studied the LiAl/LiCl-KCl/LiMn<sub>2</sub>O<sub>4</sub> cell and found an upper plateau above 2.0V but a small capacity [9]. These previous studies on the LiMn<sub>2</sub>O<sub>4</sub> cathode are all over a narrow range of discharge conditions and mainly focus on the weapon application above 400 °C. This paper presents the detailed experimental results of the LiMn<sub>2</sub>O<sub>4</sub> cathode study, and discusses its applicability to high-temperature batteries between 200 and 300 °C for borehole applications. Also, the effect of substituting Ni for Mn partly is investigated and the proper chemical compositions are proposed.

## 2. EXPERIMENTAL

### 2.1. Materials preparation

All the chemical reagents used in the experiments were analytical grade purchased from Sinopharm Chemical Reagent Co, Ltd (SCRC). A series of LiMn<sub>2-x</sub>Ni<sub>x</sub>O<sub>4</sub> (x = 0, 0.1, 0.3, 0.5) powders were synthesized through a sol-gel method using citric acid as chelating agent. The process of synthesis referred to previous work by Kunduraci and Amatucci [10]. A stoichiometric amount of reagents Li(CH<sub>3</sub>COO)·2H<sub>2</sub>O, Mn(CH<sub>3</sub>COO)<sub>2</sub>·4H<sub>2</sub>O, Ni (CH<sub>3</sub>COO)<sub>2</sub>·4H<sub>2</sub>O were dissolved in distilled water which was preheated to 75 °C and then mixed with aqueous solution of citric acid (a 1:1 mole ratio of metal ions to citric acid was chosen). After cooling to room temperature, the pH of the as-prepared solution was adjusted to neutral with aqueous ammonia. The resulting solution was mixed with a magnetic stirrer at 75 °C until a clear viscous gel occurs. The gel was then dried in a vacuum oven at 90 °C for 16h to eliminate redundant water. After being ground into powder adequately, the precursor was preliminarily annealed at 400 °C for 8 h in air. After cooling and ground again, the

resulting powder was calcined at 700 °C for 20 h, followed by cooling to room temperature along with the tube furnace.

## 2.2. Structure and morphology characterization

Thermogravimetric analysis/differential thermal analysis (TGA/DTA) was performed on a NETZSCH STA 449F3 thermal analyzer with  $\alpha$ -Al<sub>2</sub>O<sub>3</sub> as the reference substance at a heating rate of 10 °C /min. Thermal analysis was used to determine the final sintering temperature of the gel and the compatibility between cathodes and electrolytes. To identify the resulting cathodes and investigate the discharge process, XRD was performed on a Rigaku D/MAX-2200/PC diffractometer with Cu K $\alpha$  radiation, the scanning range was from 10° to 80° with a scanning speed of 4 °/min. The phases and precise lattice parameters were analyzed using JADE software (MDI). Surface morphology of the synthesized active materials was investigated using scanning electron microscopy (SEM) obtained from a Hitachi S4700 scanning electron microscope.

## 2.3. Preparation of pellets for single cell tests

The LiMgB alloy anodes (58 wt% Li, 4 wt% Mg and 38 wt% B) were obtained by punching disks (15.5 mm diameter, 0.20 g mass) from LiMgB foil. The redox potential of LiMgB/Li<sup>+</sup> is 0.001V higher than that of Li/Li<sup>+</sup>. The electrolyte binder was composed of the LiNO<sub>3</sub>-KNO<sub>3</sub> eutectic (33.2 wt% LiNO<sub>3</sub>, 66.8 wt% KNO<sub>3</sub>) mixed with 35 wt% MgO by fusing the mixture for 16 h at 300°C. The catholyte was prepared by blending 70 wt% of the active cathode material with 20 wt% electrolyte and 10 wt% graphite. Electrolyte and graphite were added necessarily to improve the ionic and electrical conductivity. The single cell each consisted of a 0.20 g LiMgB pellet and a bilayer pellet consisting of 0.30 g each of depolarizer-electrolyte (DE) and electrolyte binder (EB) layers pressed at 222 MPa. Then the two pellets were sandwiched between copper current collectors and put between heated plates in a glovebox under an atmosphere of high-purity argon (< 1 ppm each of water and oxygen). Asbestos insulations were used between single cells and heated platens to avoid any electricity contact. The discharge measurements were performed on a LAND potentiostat/galvanostat at the temperatures of 200 °C, 250 °C and 300 °C. A steady-load of 19 mA (10 mA·cm<sup>-2</sup>) was used for the galvanostatic discharge tests which fitted to the actual application conditions. The cell discharge was terminated when the voltage dropped below 1.00V.

## 3. RESULTS AND DISCUSSION

### 3.1. Material synthesis and structural characterization

Thermal properties of the LiMn<sub>2-x</sub>Ni<sub>x</sub>O<sub>4</sub> precursors obtained by a sol-gel method were studied by simultaneous TGA/DTA analyses. As thermal analysis curves of different samples present basically

consistent shapes and change rules, here we give the  $x = 0$  example to illustrate. Fig. 1 shows the simultaneous TGA/DTA curves of the  $\text{LiMn}_2\text{O}_4$  precursor.

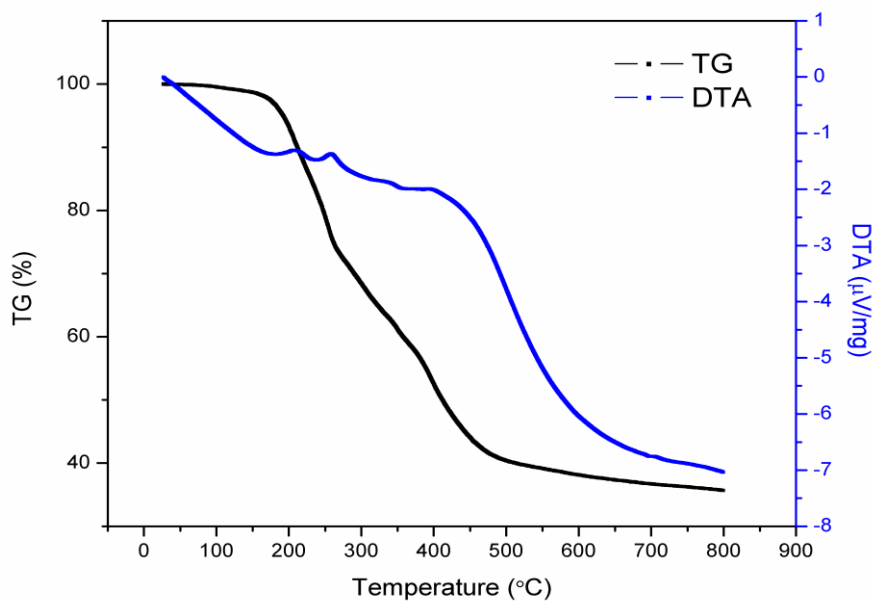


**Figure 1.** TGA/DTA curves for the  $\text{LiMn}_2\text{O}_4$  precursor obtained by a citric acid assisted sol-gel method.

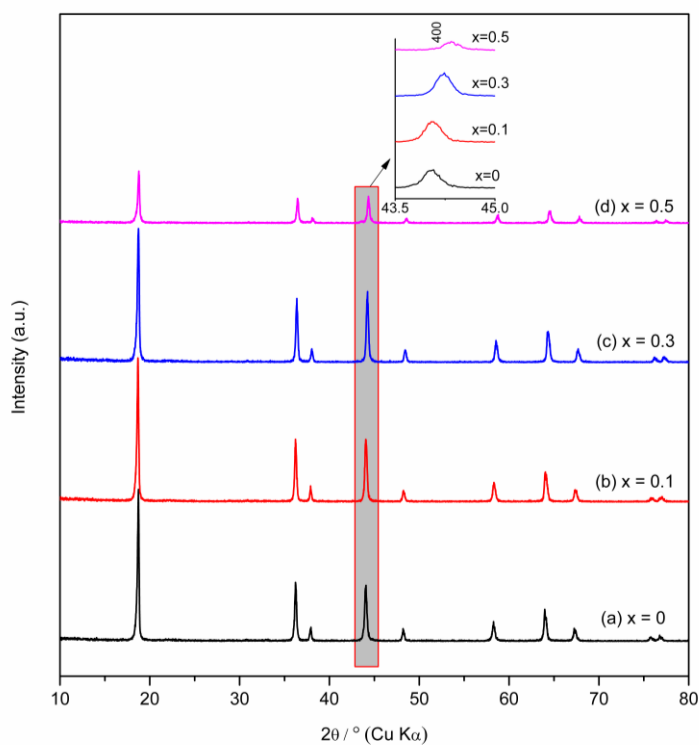


**Figure 2.** X-ray diffraction patterns of  $\text{LiMn}_{2-x}\text{Ni}_x\text{O}_4$  powders with different  $x$  values.

There is an obvious weight loss of about 60% at around 500 °C in the TG curve, which is attributed to the evaporation of residual water, the decomposition of organic matter and the generation of end-products. At temperatures of above 500 °C, there is no obvious weight loss in the TG curve and endothermic or exothermic peak in the DTA curve, which indicates the reactions have basically ended and the end-products have been obtained. In order to ensure the reactions more thorough and get better crystallinity, we set the final calcining temperature to 700 °C.

Fig. 2 shows the XRD patterns for the obtained  $\text{LiMn}_{2-x}\text{Ni}_x\text{O}_4$  powders. The XRD patterns of the four samples are quite similar with each other. As the increasing of the x value from 0 to 0.5, all samples display only a single spinel phase with a Fd3m space group without any impurity, which indicates that when the value of x is limited below 0.5, the expected single phases are obtained successfully. However, the peak position and intensity differ slightly with each other and show a certain trend. To take the (400) diffraction peak as an example, the peak position moves to right slightly as the Ni content (x) increases and the peak intensity strengthens gradually as x increases from 0 to 0.3, but a sudden diminution is observed when x reaches 0.5, that corresponds to the change of lattice parameters.

The calculated lattice parameters and unit cell volume of  $\text{LiMn}_{2-x}\text{Ni}_x\text{O}_4$  spinels on the basis of diffraction data are listed in Table 1. It can be seen that substitution manganese with nickel results in shrinkage of the lattice parameter and unit cell volume as the Ni content x increases. In original spinel  $\text{Li}_2\text{MnO}_4$ ,  $\text{Mn}^{3+}$  and  $\text{Mn}^{4+}$  with a ratio of 1:1 are uniformly distributed in the octahedral 16d sites. By the use of X-ray photoelectron spectroscopy (XPS) measurement, Aminel et al. [11] confirmed that the Ni in these compounds took oxidation state + 2 and  $\text{Mn}^{3+}$  ions were substituted by  $\text{Ni}^{2+}$ . The average oxidation state of Mn increases beyond 3.5 when substituting  $\text{Ni}^{2+}$  for  $\text{Mn}^{3+}$  to maintain electrical neutrality, that is,  $\text{Mn}^{4+}$  increases together with the decrease of  $\text{Mn}^{3+}$ . According to Zhong et al.'s research [12], the oxidation state of the  $\text{LiMn}_{2-x}\text{Ni}_x\text{O}_4$  can be written as  $\text{Li}^{+1}\text{Ni}_x^{+2}\text{Mn}_{1-2x}^{+3}\text{Mn}_{1+x}^{+4}\text{O}_4^{-2}$ . Then the average cation ionic radii of the octahedral 16d sites are calculated to be 0.5900 Å, 0.5865 Å, 0.5795 Å and 0.5725 Å respectively as the value of x increases from 0 to 0.5 ( $\text{Mn}^{3+}$  (6) = 0.65 Å,  $\text{Mn}^{4+}$  (6) = 0.53 Å, and  $\text{Ni}^{2+}$  (6) = 0.70 Å, where the number in parentheses represents the coordination number [13]), and this is why the lattice parameters decrease gradually. Also, this trend is consistent with changes of  $\text{LiMn}_{1.8}\text{Ni}_{0.2}\text{O}_4$ ,  $\text{LiMn}_{1.67}\text{Ni}_{0.33}\text{O}_4$  and so on [14]. The structural stability of the materials is improved due to the substitution of unstable  $\text{Mn}^{3+}$  with more stable Ni ions [15], which is an important factor affecting the electrochemical performance.

**Table 1.** Lattice parameters and unit cell volume of  $\text{LiMn}_{2-x}\text{Ni}_x\text{O}_4$  spinels.

Sample	Lattice parameter, a / Å	Unit cell Volume / Å <sup>3</sup>
$\text{LiMn}_2\text{O}_4$	8.22281	555.98
$\text{LiMn}_{1.9}\text{Ni}_{0.1}\text{O}_4$	8.21928	555.27
$\text{LiMn}_{1.7}\text{Ni}_{0.3}\text{O}_4$	8.19028	549.41
$\text{LiMn}_{1.5}\text{Ni}_{0.5}\text{O}_4$	8.17043	545.43

Scanning electron micrographs depicting morphological features of the  $\text{LiMn}_{2-x}\text{Ni}_x\text{O}_4$  ( $x = 0, 0.1, 0.3$  and  $0.5$ ) powders prepared at  $700\text{ }^\circ\text{C}$  are shown in Fig. 3a – d. Irregular polygon-shaped primary particles and minority bar-like shape are the main components of these samples. The grain size is estimated to be between 100 and 200 nm according to the SEM images and the mean value presents a decreasing trend gradually as Ni substitution amount  $x$  increases to 0.5, which is well consistent with XRD results.

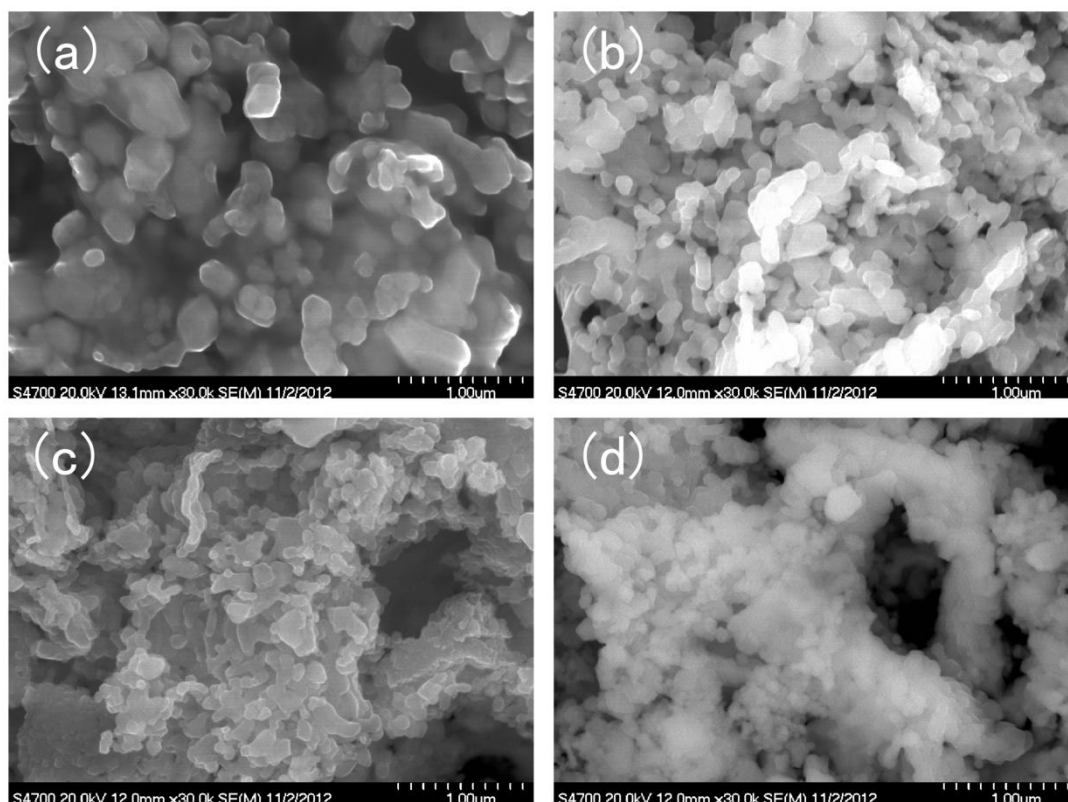


**Figure 3.** Scanning electron micrographs of (a)  $\text{LiMn}_2\text{O}_4$ , (b)  $\text{LiMn}_{1.9}\text{Ni}_{0.1}\text{O}_4$ , (c)  $\text{LiMn}_{1.7}\text{Ni}_{0.3}\text{O}_4$  and (d)  $\text{LiMn}_{1.5}\text{Ni}_{0.5}\text{O}_4$  samples.

Any high-temperature lithium battery containing severe exothermic reactions may lead to unpredictable safety problems, even thermal runaway leading to fire inside batteries. So thermal analysis was performed necessarily prior to high-temperature discharge tests to avoid any risk and eliminate any ill-suited cell combination. The compatibility of cathodes with the nitrate eutectic was examined by simultaneous TGA/DTA analyses, whose results are shown in Fig. 4a – b. It shows that in the designed temperature range of below  $300\text{ }^\circ\text{C}$ , there is no obvious weight loss and only an endothermic peak at around  $135\text{ }^\circ\text{C}$ . As the theoretical melting point of the  $\text{LiNO}_3\text{-KNO}_3$  eutectic is  $124.5\text{ }^\circ\text{C}$  [16], this endothermic peak most likely corresponds to the melting process of the eutectic. Even at an extended temperature range up to  $400\text{ }^\circ\text{C}$ , which basically reaches the upper limit temperature of the geothermal and oil/gas exploration, neither endothermic peak nor exothermic peak is observed in each DTA curve, so the safety of all the battery combinations is guaranteed commendably.

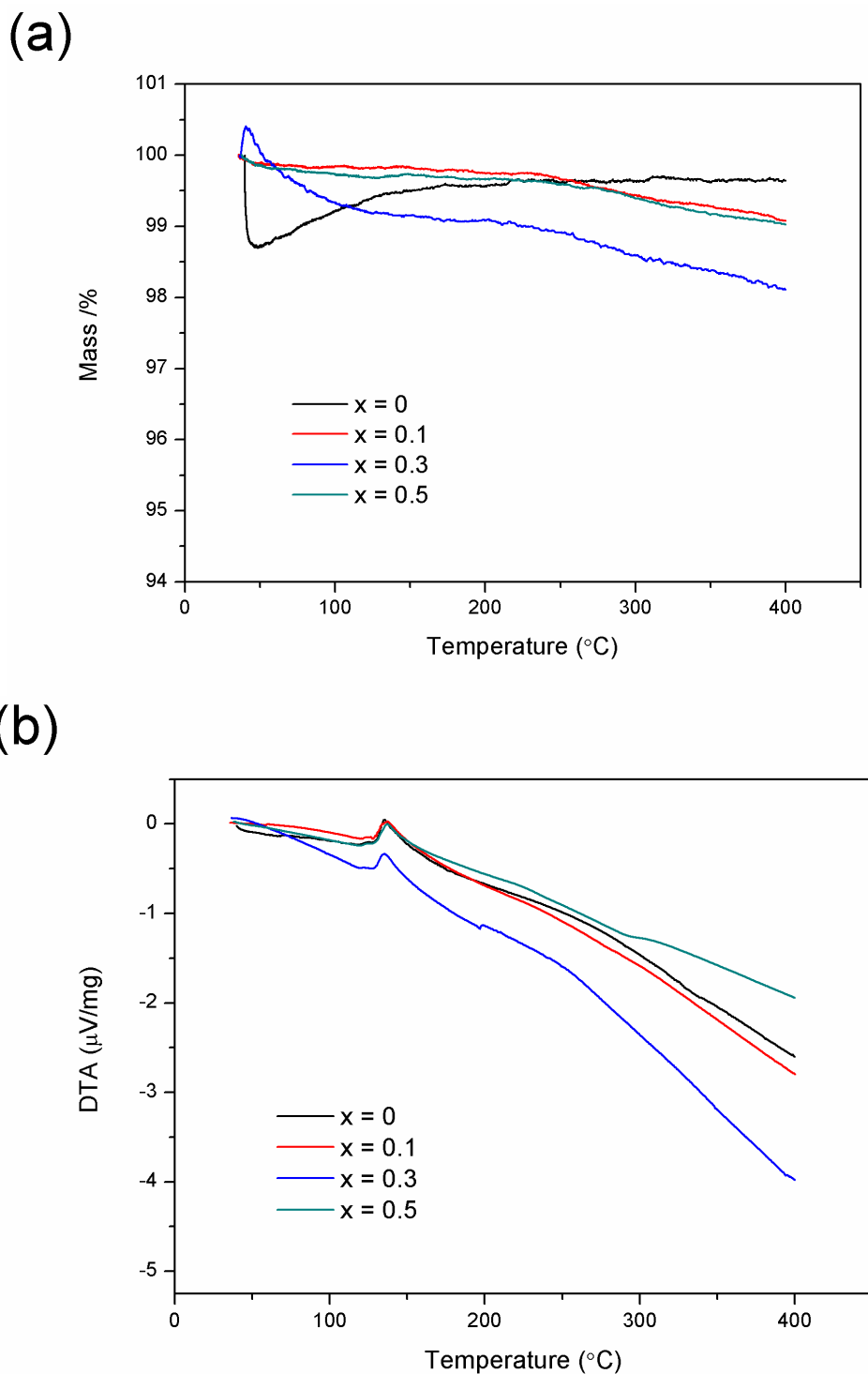


**Figure 4.** Thermogravimetric analysis and differential thermal analysis curves for the  $\text{LiMn}_{2-x}\text{Ni}_x\text{O}_4$  ( $x = 0, 0.1, 0.3, 0.5$ ) coupled with the  $\text{LiNO}_3\text{-KNO}_3$  eutectic.

### 3.2. Electrochemical performance

High-temperature discharge tests were performed on an in-house designed device as shown in Fig. 5. To take the bad kinetics of the eutectic and the existing solutions at low temperatures into consideration, we set the test temperature range to between 200 °C and 300 °C which is included in the

majority work environments of the geothermal and oil/gas exploration [1]. In order to analyze the applicability in more detail, three temperature spots, 200 °C, 250 °C and 300 °C were investigated respectively.

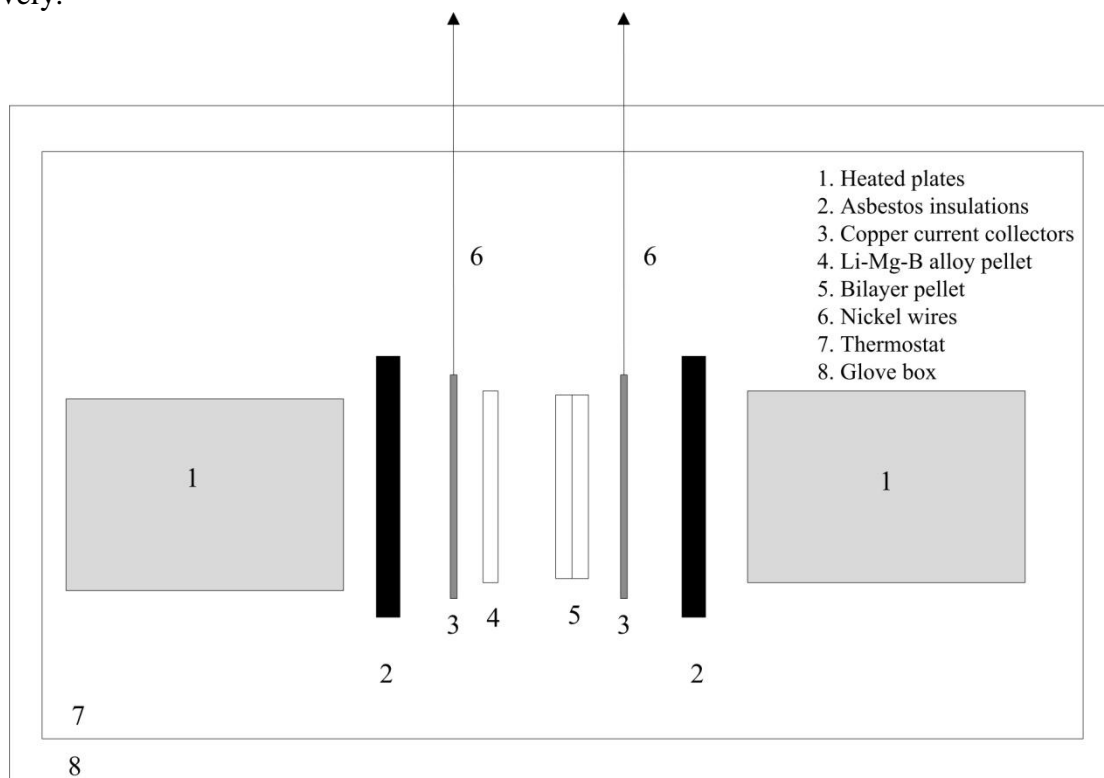


**Figure 5.** Single cell test device designed by our laboratory.

The galvanostatic discharge results for the  $\text{LiMn}_{2-x}\text{Ni}_x\text{O}_4$  at a current density of  $10 \text{ mA}\cdot\text{cm}^{-2}$  at 200 °C, 250 °C and 300 °C are presented in Fig. 6a – c and Table 2. All these single cells had an open-circuit voltage of around 2.9 V and exhibited three distinct voltage plateaux at 250 °C, which indicated a three-step process of lithium intercalation during discharge. The specific reaction mechanisms will be discussed in a later section. The incomplete and sloping plateaux at 200 °C are most possibly limited by the higher electrolyte resistance which is very strongly temperature-dependent. At relatively low temperatures close to the melting point of eutectics, the kinetics of molten salts is worse and has a significant impact on the discharge performances [17]. Serious self-discharge and polarization appeared at 300 °C, resulting from fluctuant voltage plateaux and much less capacities, especially for the  $x = 0.1$  and  $0.5$  samples. At temperatures of 200 °C and 250 °C, partial substitution of Ni for Mn significantly improved the voltage plateaux and discharge capacities. The highest capacities are  $590.95 \text{ mAh}\cdot\text{g}^{-1}$  for the  $\text{LiMn}_{1.9}\text{Ni}_{0.1}\text{O}_4$  at 200 °C and  $726.38 \text{ mAh}\cdot\text{g}^{-1}$  for the  $\text{LiMn}_{1.7}\text{Ni}_{0.3}\text{O}_4$  at 250 °C, which are much higher than those of the Ni-free sample and sulfur-based cathodes in typical thermal batteries [18, 19]. Besides the diminished capacity for the  $\text{LiMn}_{1.7}\text{Ni}_{0.3}\text{O}_4$  sample same as others at 300 °C, no obvious plateau degradation was observed in the discharge curve. So it can be concluded that the  $\text{LiMn}_{1.7}\text{Ni}_{0.3}\text{O}_4$  sample is most suitable for working in full temperature range (200 – 300 °C) due to its good electrochemical properties, especially discharge stability.

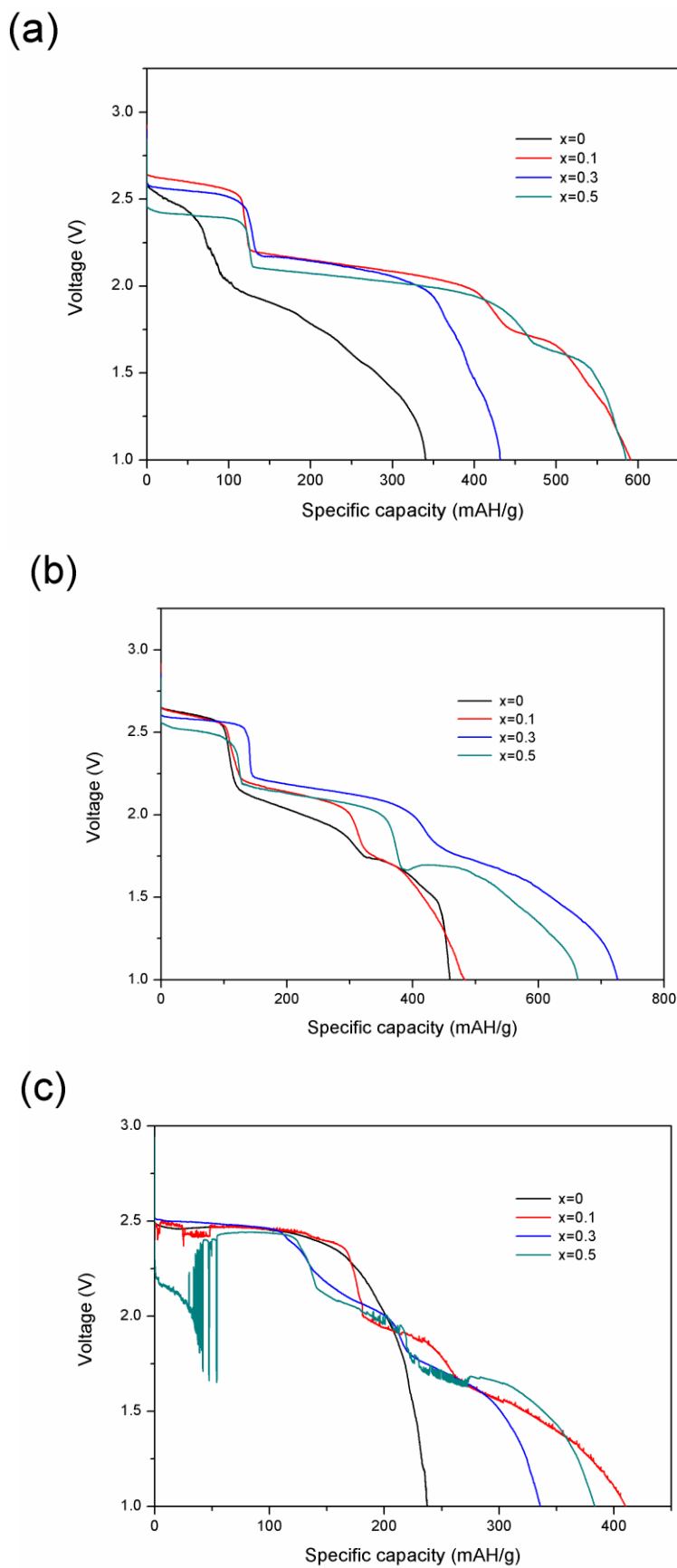


**Figure 6.** The galvanostatic discharge profiles of the Li-Mg-B/LiMn<sub>2-x</sub>Ni<sub>x</sub>O<sub>4</sub> cells at (a) 200 °C, (b) 250 °C and (c) 300 °C.

**Table 2.** The galvanostatic discharge results for the  $\text{LiMn}_{2-x}\text{Ni}_x\text{O}_4$  cathodes.

Temperature / °C	Sample	Open-circuit voltage / V	Voltage plateau / V (median of each plateau)	Unit discharge capacity / $\text{mAh}\cdot\text{g}^{-1}$ (1.00V cut-off)
200	$\text{LiMn}_2\text{O}_4$	2.9483	2.50; 1.70	340.52
	$\text{LiMn}_{1.9}\text{Ni}_{0.1}\text{O}_4$	2.9263	2.60;2.10;1.70	590.95
	$\text{LiMn}_{1.7}\text{Ni}_{0.3}\text{O}_4$	2.9018	2.55; 2.10	431.62
	$\text{LiMn}_{1.5}\text{Ni}_{0.5}\text{O}_4$	2.8454	2.40;2.00;1.60	585.29
250	$\text{LiMn}_2\text{O}_4$	2.9374	2.60;2.00;1.60	459.57
	$\text{LiMn}_{1.9}\text{Ni}_{0.1}\text{O}_4$	2.9154	2.60;2.10;1.70	483.10
	$\text{LiMn}_{1.7}\text{Ni}_{0.3}\text{O}_4$	2.8578	2.57;2.15;1.60	726.38
	$\text{LiMn}_{1.5}\text{Ni}_{0.5}\text{O}_4$	2.8299	2.50;2.10;1.70	663.19
300	$\text{LiMn}_2\text{O}_4$	2.9213	2.45	237.43
	$\text{LiMn}_{1.9}\text{Ni}_{0.1}\text{O}_4$	2.9337	2.45;1.90	410.24
	$\text{LiMn}_{1.7}\text{Ni}_{0.3}\text{O}_4$	2.8606	2.50;2.10;1.65	335.95
	$\text{LiMn}_{1.5}\text{Ni}_{0.5}\text{O}_4$	2.9412	2.45;2.00;1.65	383.43

As is shown in Fig. 6b, three distinct voltage plateaux are observed at 2.65 to 2.55V, 2.15 to 1.75V and 1.75 to 1.00V for the Ni-free spinel  $\text{LiMn}_2\text{O}_4$  at 250 °C. In order to make clear the reaction mechanisms of them, cells were discharged to 2.55V, 1.75V and 1.00V respectively, then the cathode layers were stripped and analysed by XRD. The XRD spectra before discharge and after discharge are shown in Fig. 7.

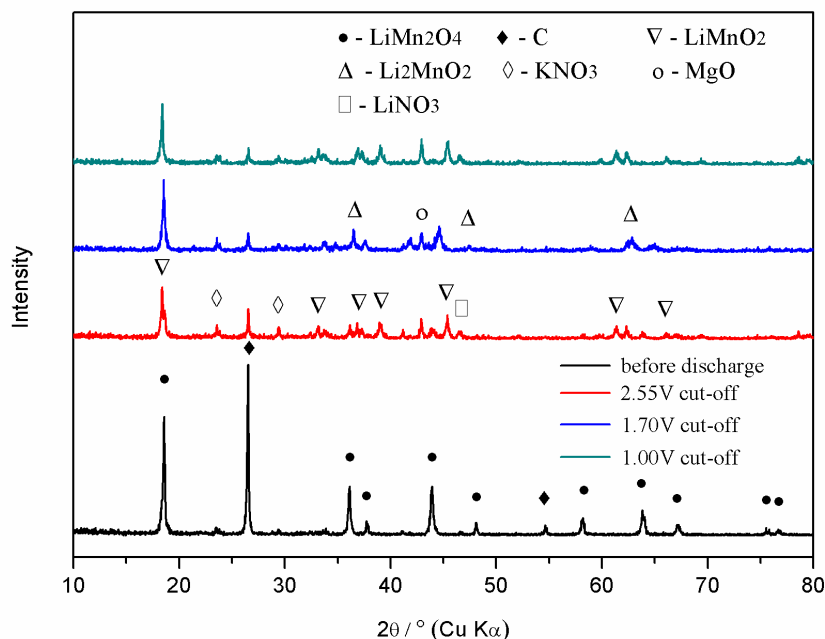


**Figure 7.** X-ray diffractograms of the starting cathode layer and partially discharged cathode layers.

The cathode material discharged to 2.55V mainly contains  $\text{LiMnO}_2$  and a small amount of unreacted  $\text{LiMn}_2\text{O}_4$  (all the additives are not be discussed). So the voltage plateau of 2.65 - 2.55V indicates that a cubic spinel phase, namely  $\text{LiMn}_2\text{O}_4$ , converts to  $\text{LiMnO}_2$  with a tetragonal spinel phase, which is similar to the case of  $\text{LiMn}_{1.5}\text{Ni}_{0.5}\text{O}_4$  at room temperature [20]. A one electron reduction process is well in accordance with the first voltage plateau, as is shown in equation 1. The theoretical discharge capacity according to this reaction is calculated to be  $147.97 \text{ mAh}\cdot\text{g}^{-1} \text{ LiMn}_2\text{O}_4$ , which fits with the actual discharge capacity of  $125.24 \text{ mAh}\cdot\text{g}^{-1} \text{ LiMn}_2\text{O}_4$ . This is equivalent to a conversion ratio of 84.6% for the  $\text{LiMn}_2\text{O}_4$  sample.



The XRD spectra of the other two discharged samples are quite similar to that of the first one only with small changes in minor peaks. Because a number of different lithiated manganese oxides share the similar XRD spectra, the reaction mechanisms of the second and third plateaux can not be determined so clearly by the method of XRD. There is a certain parallelism here between  $\text{LiMn}_2\text{O}_4$  and  $\text{Ag}_2\text{CrO}_4$  [21]. However, the possible processes can still be inferred by some evidence, such as the corresponding capacity of each plateau. The capacities relevant to the second and third plateaux are  $197.86 \text{ mAh}\cdot\text{g}^{-1}$  and  $136.47 \text{ mAh}\cdot\text{g}^{-1}$  respectively obtained from the discharge curve at 250 °C. In addition, in view of the actual conversion rate of the first step, a one electron reduction for each  $\text{LiMnO}_2$  is mostly likely responsible for the second plateau, as is shown in equation 2. In the same way, equation 3 seems most consistent with the third plateau. The conversion rates for the second and third processes are calculated to be 79.0% and 69.0% respectively. Besides, the XRD spectra do not conflict with conclusions above. So a total five electron reduction is suggested to be the reaction mechanism to a 1.00V cut-off.



#### 4. CONCLUSIONS

To explore high energy density cathode materials used in high-temperature lithium batteries for borehole applications, the spinel  $\text{LiMn}_2\text{O}_4$  was investigated in a temperature range of 200 - 300 °C along with its Ni-substituted derivatives. Synthesized with a citric acid assisted sol-gel method, one single spinel phase and small particle size were presented for each sample. Ni substitution decreased the mean particle size. The compatibility between the cathodes and the nitrate eutectic ensured the safety of the designed high-temperature lithium batteries.

The original  $\text{LiMn}_2\text{O}_4$  cathode exhibited three distinct voltage plateaux at 250 °C and the corresponding mechanisms were investigated by XRD.  $\text{LiMnO}_2$ ,  $\text{Li}_2\text{MnO}_2$  and  $\text{Li}_3\text{MnO}_2$  are suggested to be the reduction products for these three plateaux respectively together with lithium intercalation step by step.

The partial substitution of Ni for Mn improves the voltage plateaux and discharge capacities at 200 and 250 °C, the maximal specific capacity of 726.38 mAh·g<sup>-1</sup> appeared at 250 °C for the LiMn<sub>1.7</sub>Ni<sub>0.3</sub>O<sub>4</sub> sample, which surpassed most of the traditional high-temperature lithium battery cathodes. The improved structural stability is considered to be an important factor responsible for them. At a higher temperature of 300 °C, serious plateau degradation occurred except the LiMn<sub>1.7</sub>Ni<sub>0.3</sub>O<sub>4</sub>. Due to the much higher capacities than the Ni-free LiMn<sub>2</sub>O<sub>4</sub> and the discharge stability in a wider temperature range than the other substitutes, the LiMn<sub>1.7</sub>Ni<sub>0.3</sub>O<sub>4</sub> is considered as the most promising high-temperature lithium cathode material for borehole applications.

#### ACKNOWLEDGEMENT

This work was financially supported by the Scientific Research Project of Science and Technology Commission of Shanghai Municipality (09dz1206800).

#### References

1. R. A. Guidotti, F. W. Reinhardt, Judy Odinek, *J. Power Sources* 136 (2004) 257–262.
2. R. A. Guidotti, in: 35th Intersociety Energy Conversion Engineering Conference and Exhibit, 2000, p. 1276.
3. R. A. Guidotti, Patrick Masset, *J. Power Sources* 161 (2006) 1443-1449.
4. R. A. Normann, R. A. Guidotti, *Trans. Geothermal Resources Council* 20 (1996) 509.
5. M. H. Miles, in: Proc.39th Power Sources Conf., 2000, p. 560.
6. C. O. Giwa, in: Proc.35th Intern.Power Sources Symp., 1992, p. 215.
7. C. O. Giwa, *Mat.Sci.Forum*, 699 (1991) 73-75.
8. R. A. Guidotti, F.W. Reinhardt, in: Proceedings of the 39th Power Sources Conference, 2000, p. 470.
9. M. E. Bolster, R. J. Staniewicz, in: Power Sources Symposium, 1990, Proceedings of the 34th International. IEEE, 1990, p. 136.
10. M. Kunduraci, G. G. Amatucci, *J. Electrochem. Soc.* 153 (2006) A1345-A1352.
11. K. Amine, H. Tukamoto, H. Yasuda, and Y. Fujita, Abstract 70, p. 114, The Electrochemical Society Meeting Abstracts, Vol. 95-2, Chicago, IL, Oct. 8-13, 1995.
12. Qiming Zhong, Arman Bonaklarpour, Meijie Zhang, Yuan Gao, J. R. Da, *J. Electrochem. Soc.* 144 (1997) 205-213.
13. R.D. Shannon, *Acta Crystallogr.* A32 (1976) 751.
14. Seong-Ju Hwang, Hyo-Suk Park, Jin-Ho Choy, *J. Phys. Chem. B* 105 (2001) 335-342.
15. Yucheng Sun, Zhaoxiang Wang, Xuejie Huang, Liquan Chen, *J. Power Sources* 132 (2004) 161–165.
16. Ronald A. Guidotti, Frederick W. Reinhardt, in: Proc. 41st Power Sources Conf., 2004, p. 141.
17. Ronald A. Guidotti, Frederick W. Reinhardt, Judy Odinek, *J. Power Sources* 136 (2004) 257–262.
18. Patrick J. Masset, Ronald A. Guidotti, *J. Power Sources* 177 (2008) 595–609.
19. Patrick J. Masset, Ronald A. Guidotti, *J. Power Sources* 178 (2008) 456–466.
20. Kevin Rhodes, Roberta Meisner, Yoongu Kim, Nancy Dudney, Claus Daniel, *J. Electrochem. Soc.* 158 (2011) A890-A897.
21. C.O.Giwa, *Materials Science Forum* 73-75 (1991) 699-706.